

1 **Extremely high reflection of solar wind protons as neutral**  
2 **hydrogen atoms from regolith in space**

3  
4  
5 **Martin Wieser<sup>1\*</sup>, Stas Barabash<sup>1</sup>, Yoshifumi Futaana<sup>1</sup>, Mats Holmström<sup>1</sup>,**

6 **Anil Bhardwaj<sup>2</sup>, R Sridharan<sup>2</sup>, MB Dhanya<sup>2</sup>,**

7 **Peter Wurz<sup>3</sup>, Audrey Schaufelberger<sup>3</sup>,**

8 **Kazushi Asamura<sup>4</sup>**

9  
10  
11 <sup>1</sup> Swedish Institute of Space Physics, Box 812, SE-98128 Kiruna, Sweden

12 \* email: wieser@irf.se

13 <sup>2</sup> Space Physics Laboratory, Vikram Sarabhai Space Center, Trivandrum 695 022, India

14 <sup>3</sup> Physikalisches Institut, University of Bern, Sidlerstrasse 5, CH-3012 Bern, Switzerland

15 <sup>4</sup> Institute of Space and Astronautical Science, 3-1-1 Yoshinodai, Sagamihara, Japan

16  
17 **Abstract**

18 We report on measurements of extremely high reflection rates of solar wind

19 particles from regolith-covered lunar surfaces. Measurements by the Sub-keV

20 Atom Reflecting Analyzer (SARA) instrument on the Indian Chandrayaan-1

21 spacecraft in orbit around the Moon show that up to 20% of the impinging solar

22 wind protons are reflected from the lunar surface back to space as neutral

23 hydrogen atoms. This finding, generally applicable to regolith covered

24 atmosphereless bodies, invalidates the widely-accepted assumption that regolith  
25 almost completely absorbs the impinging solar wind.

26

27

## 28 **1. Introduction**

29 In the Solar System, space weathering results in most surfaces of atmosphereless bodies  
30 being covered by regolith, a layer of loose, heterogeneous material of small grain size  
31 (Clark et al., 2002). In the absence of an atmosphere, plasma interacts directly with the  
32 surface, e.g. solar wind with the lunar regolith, and it has been tacitly assumed that the  
33 plasma is almost completely absorbed (<1% reflected) in the surface material (e.g. Crider  
34 et al. 2002, Schmitt et al., 2000, Feldman et al., 2000, Behrisch & Wittmaack, 1991).  
35 Regolith reaches hydrogen saturation on a geologically very short timescale of at most  
36  $10^4$  years (Johnson & Baragiola, 1991). Once saturated, for every impinging proton a  
37 hydrogen atom is removed from the surface by sputtering, a scatter or desorption process.  
38 Here we present measurements that invalidate the widely-accepted assumption that  
39 regolith almost completely absorbs the impinging solar wind. A large fraction of up to  
40 20% is reflected as energetic neutral hydrogen atoms back to space.

41

## 42 **2. Instrumentation**

43 The Sub-keV Atom Reflecting Analyzer (SARA) instrument (Barabash et al., 2009)  
44 onboard the Indian Chandrayaan-1 spacecraft (Goswami & Annadurai, 2009) orbiting the  
45 Moon in a 100-km polar orbit measures the neutral atom flux from the lunar surface and  
46 simultaneously monitors the impinging flux of solar wind protons. The SARA instrument

47 consists of two sensors: the Solar Wind Monitor (SWIM) (McCann et al., 2007) measures  
48 solar wind ions and the Chandrayaan-1 Energetic Neutrals Analyzer (CENA) (Kazama et  
49 al., 2007) measures energetic neutral atoms (10eV-3keV) arriving from the direction of  
50 the lunar surface. Both sensors provide angular and mass resolution: SWIM has a field-  
51 of-view of  $7.5^\circ \times 180^\circ$  divided into 16 angular pixels covering directions from nadir to  
52 zenith on the sun facing side of the spacecraft. The orbital motion of Chandrayaan-1 is  
53 used to scan the SWIM field-of-view across the full solar wind angular distribution. The  
54 center of the CENA field-of-view is nadir-pointing and in total  $160^\circ$  cross-track times  $7^\circ$   
55 along-track in size, divided into 7 angular pixels. Mass resolution  $m/dm$  of both sensors is  
56 2-3, depending on sensor, angular pixel and mass. The geometric factor for SWIM is  $5$   
57  $\cdot 10^{-5} \text{ cm}^2 \text{ sr eV/eV}$  for 500 eV protons. The geometric factor of CENA is  $5 \cdot 10^{-8} \text{ cm}^2 \text{ sr}$   
58  $\text{eV/eV}$  for 500eV neutral hydrogen. Both values are for a single angular pixel at the  
59 center of the field-of-view.

60

### 61 **3. Observations**

62 During nominal solar wind conditions SARA observed that up to 16-20% of the proton  
63 flux impinging on the lunar surface is reflected back to space as energetic neutral  
64 hydrogen atoms. SARA persistently detects high intensity fluxes of energetic neutral  
65 hydrogen atoms propagating from the lunar surface while the latter is illuminated by the  
66 solar wind. The reflected neutral atom flux changes consistently with the change in solar  
67 wind incident angle (Figure 1), with the reported numbers reached at the lunar equator.  
68 No significant energetic neutral atom flux is observed on the night side. As the intensity

69 of the impinging solar wind proton flux changed orbit by orbit, the intensity of the  
70 reflected neutral atom flux changed correspondingly and consistently (Figure 2). The  
71 reflected neutral hydrogen that was observed has an energy spectrum with a distinct  
72 upper energy of 300 eV, roughly half of the measured central energy (540 eV) of the  
73 impinging protons. Upon reflection from the surface, solar wind particles experience an  
74 average energy loss of more than 50%.

75

#### 76 **4. Discussion and Conclusions**

77 Ions with solar wind energies interacting with surfaces are likely to be neutralized e.g. by  
78 resonant or Auger neutralization, before being absorbed or reflected (e.g. Niehus et al.,  
79 1993). We observe that up to 20% of solar wind protons are reflected from the lunar  
80 surface back to space as energetic neutral hydrogen atoms with energies larger than 25  
81 eV (Figure 2). This high reflection invalidates the previous assumption that regolith  
82 almost completely absorbs the impinging solar wind. On a saturated surface the sum of  
83 all loss processes equals the solar wind precipitation, the high reflection yield reduces  
84 thus the amount of hydrogen available for release by other processes, such as sputtering  
85 or desorption, both mechanisms predominantly producing neutrals with energies of only  
86 a few eV (Betz & Wien, 1994). Since the energy of the reflected energetic neutral  
87 hydrogen is much higher than the escape energy, escaping atoms propagate on ballistic  
88 trajectories. They can be used for detailed remote imaging of the solar wind–surface  
89 interaction (Bhardwaj et al., 2005, Futaana et al., 2006). The average energy loss of more  
90 than 50% when interacting with the surface is likely due to several mechanisms. A simple  
91 classical binary collision model (Niehus et al, 1993) gives an energy loss between 10%

92 and 20%. This indicates the presence of other loss mechanisms, such as multiple  
93 scattering processes or interaction with the crystal lattice. Another possible loss process is  
94 retarding of impinging solar wind ions by a positive surface potential on the dayside  
95 (Vondrak, 1992), before the ions interact with the regolith surface. The observed lunar  
96 energetic neutral hydrogen component with an energy of up to 300eV should also be  
97 visible in measurements of Doppler-shifted Lyman alpha emissions (Gott & Potter,  
98 1970). The rate of implantation of solar wind  $^4\text{He}$  and  $^3\text{He}$  in the lunar regolith has to be  
99 reconsidered as well, because it can be expected that helium will have a similar reflection  
100 rate to hydrogen. Helium ions are efficient in creating hydrogen recoils when impinging  
101 on the surface (Niehus et al., 1993), a process that will additionally remove hydrogen  
102 from the lunar surface. It is expected that high solar wind reflection occurs on similar  
103 bodies in the Solar System as well, e.g. on Mercury, planetary satellites such as Phobos or  
104 Deimos, or on asteroids. Finally, the high neutral hydrogen reflection implies a lower  
105 hydrogen implantation rate in the regolith. Earlier work on the hydrogen influx on the  
106 lunar surface assumed almost complete absorption of solar wind ions (Crider et al. 2002,  
107 Schmitt et al., 2000, Feldman et al., 2000, Behrisch & Wittmaack, 1991), a finding which  
108 has to be revisited in the light of the present results: in equilibrium conditions, escaping  
109 and trapped hydrogen must equal the impinging hydrogen from solar wind. The efficient  
110 reflection process reduces the possible trapping rate e.g. at the lunar poles. This makes it  
111 less likely that hydrogen at the poles is entirely of solar wind origin.

112

113

114

115 **References**

116

117 Barabash, S., A. Bhardwaj, M. Wieser, R. Sridharan, T. Kurian, S. Varier, E.

118 Vijayakumar, V. Abhirami, K. V. Raghavendra, S. V. Mohankumar, M. B. Dhanya, S.

119 Thampi, K. Asamura, H. Andersson, Y. Futaana, M. Holmstrom, R. Lundin, J.

120 Svensson, S. Karlsson, R. D. Piazza, P. Wurz, Investigation of the solar wind-Moon

121 interaction onboard Chandrayaan-1 mission with the SARA experiment, Current

122 Science, 96, 4, 526 (2009)

123 Behrisch, R. and K. Wittmaack, "Introduction" in Sputtering by Particle Bombardment

124 III, ed. R. Behrisch and K. Wittmaack, pp. 1-13, Springer-Verlag, New York, 1991.

125 Betz, G. and K. Wien, Energy and angular distributions of sputtered particles, Int. J.

126 Mass Spec. and Ion Proc. 141, (1994)

127 Bhardwaj, A., S. Barabash, Y. Futaana, Y. Kazama, K. Asamura, R. Sridharan, M.

128 Holmström, P. Wurz, and R. Lundin, Low Energy Neutral Atom Imaging on the Moon

129 with the SARA Instrument aboard Chandrayaan-1 Mission, Journal of Earth System

130 Sciences, 114 (No.6), 749-760 (2005)

131 Clark, B. E., B. Hapke, C. Pieters, D. Britt, Asteroid Space Weathering and Regolith

132 Evolution, Asteroids III, eds. W. F. Bottke Jr., A. Cellino, P. Paolicchi, and R. P.

133 Binzel, University of Arizona Press, Tucson, (2002) 585-599.

134 Clementine image data available at <http://www.cmf.nrl.navy.mil/clementine/>.

135 Crider, D.H., and R.R. Vondrak, Hydrogen migration to the lunar poles by solar wind  
136 bombardment of the moon, *Advances in Space Research*, Volume 30, Issue 8, October  
137 2002, Pages 1869-1874

138 Feldman, W.C., D.J. Lawrence, R.C. Elphic, B.L. Barraclough, S.Maurice, I. Genetay,  
139 and A.B. Binder, Polar Hydrogen deposits on the Moon, *Journal of Geophysical*  
140 *Research*, Volume 105, Issue E2, p. 4175-4196 , 02/2000

141 Futaana, Y., S. Barabash, M. Holmström, and A. Bhardwaj, Low energy neutral atoms  
142 imaging of the Moon, *Planet. Space Sci.* 54, 132-143, 2006.

143 Goswami, J. N., and M. Annadurai, Chandrayaan-1: India's first planetary science  
144 mission to the moon, *Current Science*, 96, 4, 25 February 2009

145 Gott, J. R., A.E. Potter Jr., Lunar Atomic Hydrogen and Its Possible Detection by  
146 Scattered Lyman- $\alpha$  Radiation, *Icarus* 13, 202--206 (1970)

147 Johnson, R.E. and R. Baragiola. Lunar Surface: Sputtering and Secondary Ion Mass  
148 Spectrometry, *Geophys. Res. Lett.*, 18, 2169, 1991.

149 Kazama, Y., S. Barabash, M. Wieser, K. Asamura, and P. Wurz, Development of an  
150 LENA instrument for planetary missions by numerical simulations, *Planet. Space Sci.*  
151 55 (2007) 1518-1529.

152 McCann, D., S. Barabash, H. Nilsson, and A. Bhardwaj, Miniature Ion Mass Analyser,  
153 *Planetary and Space Science*, 55 (No.9), 1190-1196 (2007).

154 Niehus, H., W. Heiland, E. Taglauer, Low-energy ion scattering at surfaces, Surface  
155 Science Reports 17 (1993) 213-303

156 Schmitt, H.H., G. L. Kulcinski, J. F. Santarius, J. Ding, M. J. Malecki, and M. J.  
157 Zalewski, Solar-Wind Hydrogen at the Lunar Poles, Proceedings of Space 2000: the  
158 seventh international conference and exposition of engineering, construction,  
159 operations, and business in space, February 27 - March 2, 2000, in Albuquerque, New  
160 Mexico, USA, pp. 653-660, (doi 10.1061/40479(204)79)

161 Vondrak, R. R., Lunar base activities and the lunar environment. Proceedings of the 2nd  
162 Conference on Lunar Bases and Space Activities. NASA Johnson Space Center,  
163 September 1992, Volume 1, pp. 337-345 (SEE N93-17414 05-91),  
164 1992lbsa.conf..337V

165

165 **Legends**

166 **Figure 1:** Neutral hydrogen measurements recorded during three consecutive orbits on 6  
167 February 2009. The flux from the surface seen with the nadir-looking sensor pixel is  
168 shown by thin colored zenith-pointing lines. Data from all three orbits covering an area  
169 around 8° W lunar longitude on the lunar dayside are superimposed. Color and the line  
170 length depict the flux intensity. Solar wind ions impinge onto the lunar surface  
171 approximately from the Sun direction indicated by the green axis. A clear dependence of  
172 the flux on solar zenith angle is seen on the dayside. Small fluxes on the night side  
173 correspond to the instrument background. The lunar surface map is taken from  
174 Clementine image data.

175 **Figure 2:** Energy spectra of the solar wind (right side, open squares) and of the  
176 corresponding reflected energetic hydrogen (left side, open circles). Data from the same  
177 three orbits on 6 February 2009 as used in Figure 1 are shown, with dayside equator  
178 crossings at 05:22 UTC (solid lines), 07:20 UTC (dashed lines) and 09:18 UTC (dotted  
179 lines). Measurements were taken shortly after the Moon crossed the Earth's bow shock to  
180 the downstream direction, resulting in a broadening of the energy spectrum of the solar  
181 wind protons. Note the good correlation between the reflected energetic neutral flux and  
182 the solar wind flux variations. The reflection yield when crossing the equator is 0.16 to  
183 0.20, depending on the orbit. Taking uncertainties arising from detector efficiency into  
184 account and assuming an isotropic angular scatter distribution of the energetic hydrogen  
185 atoms, the average values over several orbits are, with 95% confidence, between 0.03 and  
186 0.35. The isotropic angular scattering distribution on the surface assumed for calculating  
187 the total reflected flux is based on data obtained from pixels looking in non-nadir

188 directions. Error bars shown represent knowledge of the instrument geometric factor ( $1\sigma$ ).

189

190

191

192

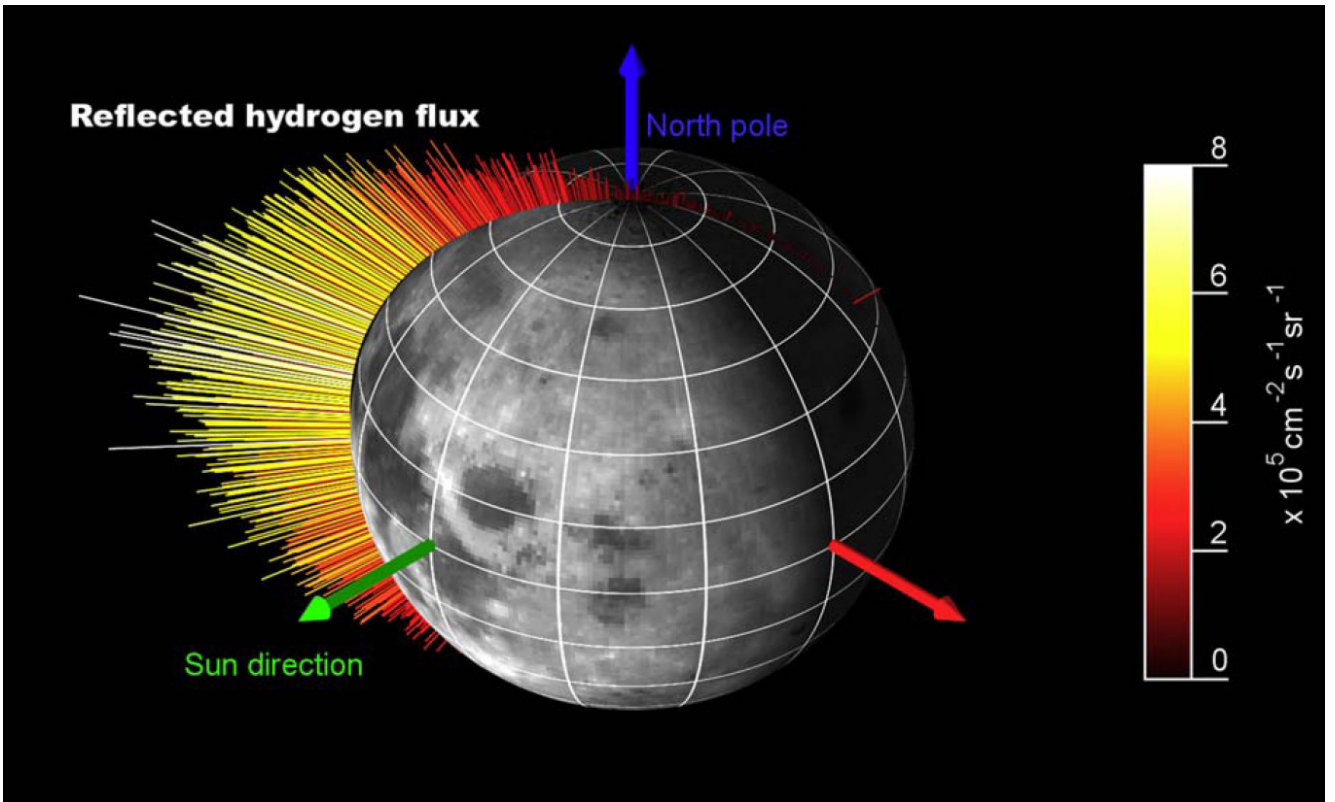


Figure 1

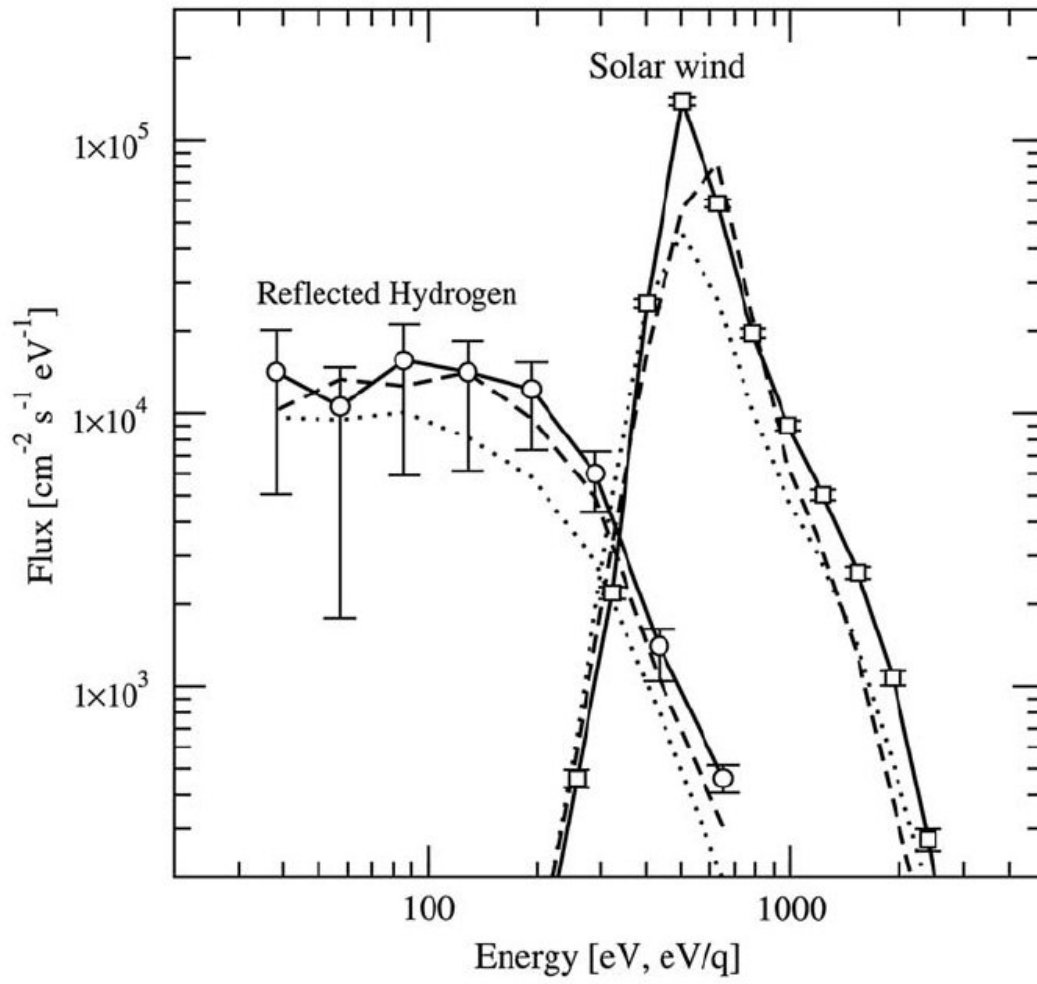


Figure 2